



Microbubble Measurements using Image Processing with the YOLOv8 Comparison Model

James Julian^{1*}, Faiz Daffa Ulhaq², Annastya Bagas Dewantara², Riki Hendra Purba¹, Fitri Wahyuni¹, Thomas Junaedi³

¹ Department of Mechanical Engineering, Faculty of Engineering, University of Pembangunan Nasional Veteran, Jakarta 12450, Indonesia

² Department of Electrical Engineering, Faculty of Engineering, University of Pembangunan Nasional Veteran, Jakarta 12450, Indonesia

³ Faculty of Engineering, Universitas Muhammadiyah Jakarta, Indonesia

ARTICLE INFO

JASAT use only:

Received date : 30 January 2024

Revised date : 25 February 2024

Accepted date : 27 May 2024

Keywords:

Microbubble,
Image Processing,
YOLOv8,
Matrix Evaluation.

ABSTRACT

Gas-liquid two-phase is a situation where the gas phase of a liquid coexists together. The presence of gas that forms a region in the liquid environment causes the formation of bubble flow. The parameters of the bubble flow carry important information about the behavior and characteristics of the bubble. This research was carried out by detecting the size and area of the bubble using YOLOv8-based image processing by comparing the model's performance to produce improvements in inference time, increase accuracy, and reduce computational load. Bubble images were collected by adding 0.4 mm copper wire as a comparison to convert mm to pixels; then, the images were labeled and trained with various YOLOv8 models. Confusion matrix, precision and recall are used as comparative evaluation materials for the YOLOv8 model to obtain good model performance. In this study, the AUC of the Precision and Recall curve closest to the value 1 is the YOLOv8m model of 0.990. The comparison results of the matrix evaluation with the best model are the YOLOv8m model with mAP of 99.00% and F1-score of 96.86%. Microbubble measurements are calculated from the output of the YOLOv8 model by converting pixel units to mm. The model used in bubble measurements is the model with the best evaluation results and the model that gets the smallest radius value by considering measurement uncertainty, namely YOLOv8m with a minimum radius of 0.66 ± 0.04 mm..

© 2024 Journal of Applied Science and Advanced Technology. All rights reserved

Introduction

Gas-liquid two-phase is a situation where the gas phase of a liquid coexists together. The presence of gas that forms a region in the liquid environment causes the formation of bubble flow. Detected bubble parameter information is often used to identify flow and mass transfer characteristics, flow regime, pressure drop, and heat transfer, which makes bubble flow important in the study and domains of chemical engineering, materials science, and geophysics.

The parameters of the bubble flow carry important information about the behavior and characteristics of the bubble. The size of the bubble indicates lower gas flow rates or higher liquid viscosity [1], the

shape of the bubble indicates the presence of flow turbulence or obstacles in the path [2], and the frequency and speed of the bubbles indicate the heat and mass transfer rates of the flow [3].

Various methods are used to detect the characteristics of each of these parameters. Quoc et al. used three capacitive electrodes to measure the volume of bubbles which were detected from the voltage readings of each electrode [4], the readings produced from the electrode sensor were susceptible to electromagnetic interference (EMI) as well as parasitic capacitance from the printed circuit board (PCB). Haas et al. used Faster-Region based Neural Network (Faster-RCNN) to measure the length and width of each bubble as well as segmentation to determine the size of the bubble from high-speed camera readings [5], however using Faster-RCNN for localizing the position of the bubble and adding a Convolutional Neural Network (CNN) as shape

* Corresponding author.

E-mail address: zames@upnvi.ac.id

regression has a large computational burden and a longer inference time. Andruszkiewicz et al. used the ultrasound transit time technique to measure the fluid velocity of bubbles in liquid-metal-gas-flow [6]. However, detection with this method requires complex equipment set-up, which is challenging to carry out.

To overcome this problem, this research aimed to detect the size and area of bubbles using YOLOv8-based localization objects to improve inference time, increase accuracy, and reduce computational load. The prediction system is modeled based on a computer modeling program. Model performance is determined using various evaluation metrics to determine the model's performance in measuring the bubble shape as an object for detection.

Methods

This research aims to obtain the microbubble size through image processing methods by focusing on the performance comparison of the YOLOv8 model, which will be discussed in detail in the following section. The image processing method was chosen to identify and measure microbubbles' size accurately. The data needed in this research was collected using a mirrorless camera to capture images of bubbles in a mini aquarium. The pump aerator produces bubbles, and then a 0.4 mm copper wire is dipped, which is used as a converter from mm to pixels and also functions as a comparison for the bubble size. Comparative calculations between bubble and copper wire will be used to determine the pixel scale in image processing.

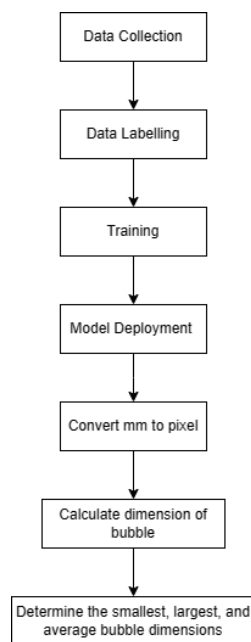


Figure 1. Flow diagram for microbubble detection

This study captured 21 microbubble image data by a mirrorless camera, which was then collected and annotated. The annotation process begins by providing a name and label. The annotated data set is then loaded in the file system which is downloaded to the local file system.

a. YOLOv8

YOLOv8 is a deep learning-based object detection model which results from optimization and development of the previous version of the YOLO series. YOLOv8 has a similar architecture to YOLOv5 by modifying YOLOv5's CSPDarknet by using Feature Pyramid Network (FPN) and Path Aggregation Network (PAN) [7] and using Complete Intersection Over Union (CIoU) as loss functions for bounding box, which uses aspect ratio as a consideration for providing a penalty for error [8], as well as Distribution Local Focus (DLF) by giving different weights to different eras based on the distribution of objects in the image which is based on the probability of the location of objects divided into the image region [9].

In the preprocessing part of YOLOv8, the image synthesis method with mosaic augmentation is carried out by creating a new image, a combination of many images to prevent overfitting and increase the model's accuracy [10]. The input of the model is an image that has been annotated with the location of the bounding boxes and classes of predicted images.

b. Evaluation Matrix

In assessing the extent to which the trained detection model is successful, we evaluate various metrics, such as Confusion Matrix, Mean Average Precision (mAP), Precision-Recall Curve, and F1-score which are common metrics in object detection tasks. The term mAP (0.5) refers to the average precision above the Intersection over Union (IoU) threshold of 0.5, while mAP (0.5 – 0.95) is the average of mAP calculated at various IoU thresholds, ranging from 0.5 to 0.95 with an increasing interval of 0.05 [11], [12]. Mean average precision (mAP) is defined as follows:

$$AP_i = \frac{TP}{TP+FP} \quad (1)$$

$$mAP = \frac{1}{N} \sum_{i=1}^N AP_i \quad (2)$$

In the object detection task, test results can be grouped into four categories, namely true positive (TP), true negative (TN), false positive (FP), and false negative (FN). In this case, TP represents a bounding box with a correctly identified target

bubble. FP represents a bounding box that is incorrectly identified as a bubble. FN shows the target is not identified as a bubble, and no bounding box has been drawn. Based on this, precision, recall, and F1-score are used for evaluation, as shown in equations (3) – (5).

$$precision = \frac{TP}{TP+FP} \quad (3)$$

$$recall = \frac{TP}{TP+FN} \quad (4)$$

$$F1 - score = \frac{2 \times precision \times recall}{precision + recall} \quad (5)$$

Precision is defined as the proportion of samples that are categorized as positive to all samples that are correctly identified. The recall ratio is a measure of how many positive samples are successfully categorized in the classifier compared to all positive samples [13]. To measure model accuracy, the F1-score considers recall and precision, then tries to adjust them by giving more weight to false negatives and false positives while ignoring many true negatives [14], [15].

c. Microbubble

Bounding boxes are used on the microbubble dataset to label microbubble images. They play an important role in image processing models, which can measure the size, proportion, and location of objects accurately based on the information provided by the bounding box [16]. A bounding box classifies each pixel of an image in an area bounded by the location represented by pixel coordinates (x, y) to distinguish pixels that belong to the same category according to the corresponding target [17].

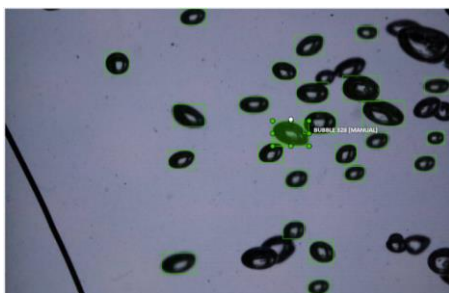


Figure 2. Bubble Labelling

The method used to determine the size of the bubble produced by the pump is to compare the bubble with a 0.4 mm copper wire. The bubble dimensions are calculated by comparing the original wire size with the pixel size as shown in equation (6). The wire width in mm is converted to pixels using the Pythagorean formula because the position of the

wire forms a right triangle in pixels, as in equation (7), with r is the radius of the copper wire in pixel.

$$\frac{1 \text{ px}}{x \text{ mm}} = \frac{r \text{ px}}{0.4 \text{ mm}} \quad (6)$$

$$r = \sqrt{L_{wire}^2 + W_{wire}^2} \quad (7)$$

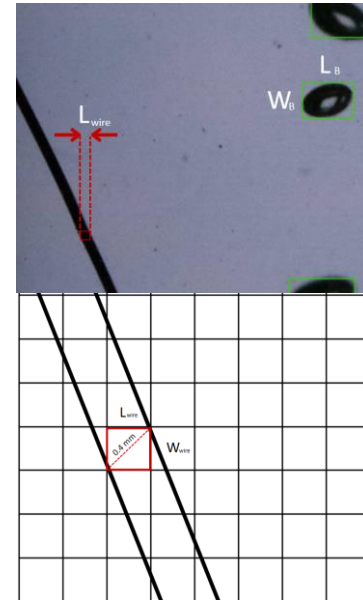


Figure 3. Microbubble movement conversion from image

The number of bubbles detected can be determined by counting the bounding boxes. After knowing the size and number of microbubbles detected, calculations can be made for the maximum and minimum size values. The average is calculated using equations (8) – (10) from the overall size of the microbubbles detected.

$$r_{mean} = \frac{\sum_{i=1}^n r_n}{n} \quad (8)$$

$$r_{min} = \min(n) \quad (9)$$

$$r_{max} = \max(n) \quad (10)$$

d. Uncertainty Level

Uncertainty is an important method in calculating measurements to reduce various factors that cause measurement errors. Uncertainty in measurements can determine the accuracy of measurement results which require more precision [18]. Uncertainty calculations involve standard deviation and average measurements. Analysis is carried out to find the level of measurement uncertainty. The level of uncertainty can be used as an indicator of aspects of measurement reliability [19]. Calculating uncertainty using standard deviation is shown in equations (11) – (13).

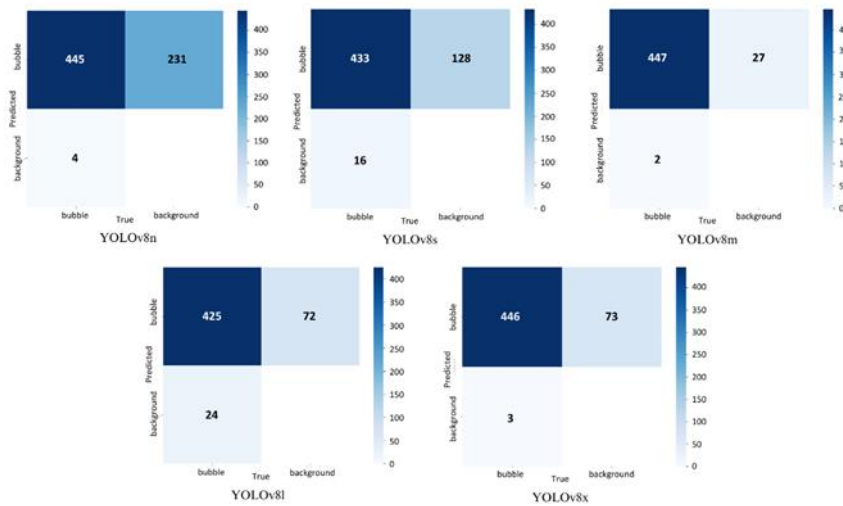


Figure 1. Confusion Matrix

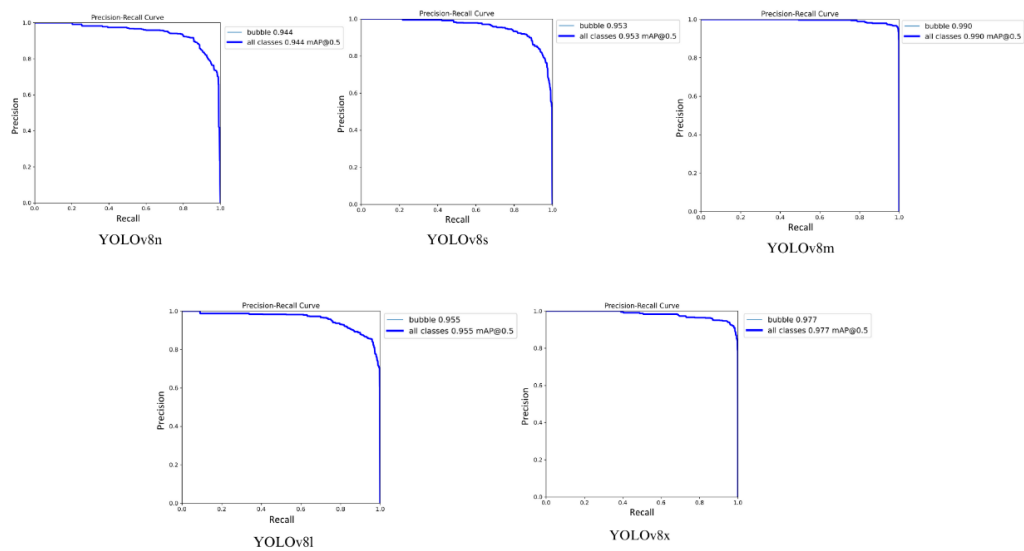


Figure 2. Precision and Recall Curve

$$\sigma^2 = \frac{\sum(x_i - \mu)^2}{n} \quad (11)$$

$$\sigma = \sqrt{\frac{1}{n} \sum_{i=1}^n (x_i - \mu)^2} \quad (12)$$

$$\sigma_x = \frac{\sigma}{\sqrt{n}} \quad (13)$$

Results and Discussions

The training program is based on Python-3.11.4 (based on pytorch-2.0.1). The simulation tools used in this experiment are NVIDIA GeForce RTX 4060. The YOLO models that were trained, namely YOLOv8n, YOLOv8s, YOLOv8m, YOLOv8l, and YOLOv8x, were carried out by testing the data that had been collected to determine the best model by considering the test results based on matrix evaluation.

a. YOLO Model of Microbubble Detection

A comparison of the confusion matrix between models is shown in Figure 4. The models that have been created are divided into different classes; in this case, the class is a bubble. The picture shows that the YOLOv8m model has the largest True Positive value, 447. In this case YOLOv8m can correctly detect the largest bubble, which is classified as a bubble, but it only has a value of 2 for True Negative, where our model cannot detect bubbles. This can be interpreted as our model being sufficient to detect bubbles well.

The precision and recall curves are used as more objective indicators to evaluate model performance, consisting of precision on the vertical axis and recall on the horizontal axis. In this research, IoU 0.5 is used as the bubble threshold. The higher the AUC of

the Precision and Recall curve, the better the model's ability to differentiate between positive and negative classes, and the closer the curve value is to 1, the better the model's performance. In this study, the AUC of the Precision and Recall curve closest to the value 1 is the YOLOv8m model of 0.990, as shown in Figure 5.

To get good bubble detection results, in this paper we choose YOLOv8 as the latest version by comparing models, namely YOLOv8n, YOLOv8s, YOLOv8m, YOLOv8l, and YOLOv8x. These experiments use the same tools, datasets, and methods, while maintaining the same proportions between training and testing sets. Comparative data between models with mAP, precision, recall, and F1-score matrix evaluations are presented in Figure 6.

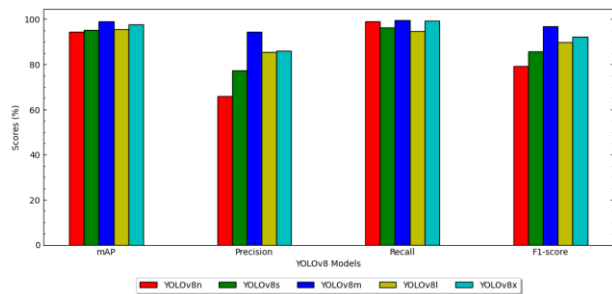


Figure 3. Comparison of the YOLOv8 model on the bubble dataset

It can be observed in Figure 6 that the best model with the largest mAP is the YOLOv8m model at 99.00% and continued by YOLOv8x (97.70%), YOLOv8l (95.50%), YOLOv8s (95.30%), and YOLOv8n (94.40%). Not only that, YOLOv8m also produced the highest F1-score of 96.86%, this indicates that the accuracy of the model evaluation results is very good. Without a doubt, the YOLOv8m model can also increase precision in bubble detection and in line with the research conducted by Kumari et al which shows that YOLOv8m is the better model to achieve high precision [20], whereas, in this paper, we need high precision to get precise bubble measurements.

b. Microbubble Measurement

The bubble detection output from each model provides bubble measurement results, which are then converted from pixels to mm. Bubble measurements are calculated, considering uncertainty to increase confidence and optimize measurement results. Uncertainty is calculated by involving the standard deviation of each measurement in each model tested, as presented in Figure 7.

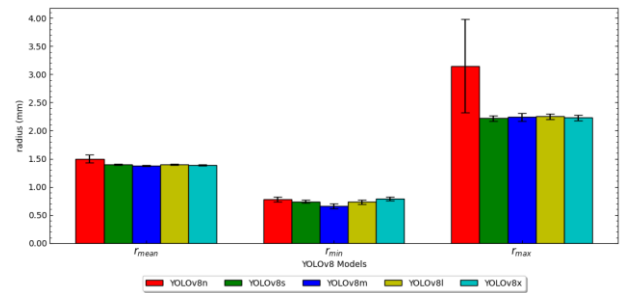


Figure 4. Comparison of YOLOv8 models on measurement data

Figure 7 shows that the smallest possible bubble size is needed to get microbubbles. Therefore, we will focus on the smallest r bubble value on the minimum radius bar graph. The YOLO model with the smallest minimum radius value is given by the YOLOv8m model of 0.66 ± 0.04 mm.

Conclusions

Based on the research and testing that has been carried out, it was found that the YOLOv8m model is the model with the best performance, which was obtained based on the AUC of the Precision and Recall curve, which is closest to the value 1, namely the YOLOv8m model of 0.990 and matrix evaluation results with mAP of 99.00% and F1-score of 96.86%. The YOLOv8 model output provides microbubble measurement results converted from pixels to mm using the standard deviation of the microbubble measurement uncertainty. YOLOv8m gets the smallest minimum radius value compared to other models, 0.66 ± 0.04 mm. Therefore, the best-performing YOLOv8m model can be used to perform microbubble measurements.

Acknowledgment

Thank you to all the authors who participated and contributed to the publication of this scientific work.

Author Contributions

The authors' contributions to the paper are as follows: study conception, design, analysis, and interpretation of results: James Julian, Faiz Daffa Ulhaq, Annastya Bagas Dewantara; data collection: Riki Hendra Purba, Fitri Wahyuni; draft manuscript preparation: Thomas Junaedi. All authors have reviewed the results and approved the final version of the manuscript.

Conflicts of Interest

All authors declare that they have no conflicts of interest.

References

- [1] D. W. Moore, "The velocity of rise of distorted gas bubbles in a liquid of small viscosity," *J Fluid Mech*, vol. 23, no. 4, pp. 749–766, 1965, <https://doi.org/10.1017/S0022112065001660>
- [2] D. Eskin, E. Meretskaya, and A. Vikhansky, "A model of breakup of a rising bubble in a turbulent flow," *Chem Eng Sci*, vol. 226, p. 115846, Nov. 2020, <https://doi.org/10.1016/j.ces.2020.115846>
- [3] G. H. Yeoh and J. Y. Tu, "Numerical modelling of bubbly flows with and without heat and mass transfer," *Appl Math Model*, vol. 30, no. 10, pp. 1067–1095, Oct. 2006, <https://doi.org/10.1016/j.apm.2005.06.012>
- [4] T. Vu Quoc, H. Nguyen Dac, T. Pham Quoc, D. Nguyen Dinh, and T. Chu Duc, "A printed circuit board capacitive sensor for air bubble inside fluidic flow detection," *Microsystem Technologies*, vol. 21, no. 4, pp. 911–918, Apr. 2015, <https://doi.org/10.1007/s00542-014-2141-8>
- [5] T. Haas, C. Schubert, M. Eickhoff, and H. Pfeifer, "BubCNN: Bubble detection using Faster RCNN and shape regression network," *Chem Eng Sci*, vol. 216, p. 115467, Apr. 2020, <https://doi.org/10.1016/j.ces.2019.115467>
- [6] A. Andruszkiewicz, K. Eckert, S. Eckert, and S. Odenbach, "Gas bubble detection in liquid metals by means of the ultrasound transit-time-technique," *The European Physical Journal Special Topics* 2013 220:1, vol. 220, no. 1, pp. 53–62, Mar. 2013, <https://doi.org/10.1140/epjst/e2013-01796-0>
- [7] D. Reis, J. Kupec, J. Hong, and A. Daoudi, "Real-Time Flying Object Detection with YOLOv8," May 2023, Accessed: Feb. 21, 2024. [Online]. Available: <https://arxiv.org/abs/2305.09972v1>
- [8] Z. Zheng, P. Wang, W. Liu, J. Li, R. Ye, and D. Ren, "Distance-IoU Loss: Faster and Better Learning for Bounding Box Regression," *Proceedings of the AAAI Conference on Artificial Intelligence*, vol. 34, no. 07, pp. 12993–13000, Apr. 2020, <https://doi.org/10.1609/aaai.v34i07.6999>
- [9] X. Li *et al.*, "Generalized Focal Loss: Learning Qualified and Distributed Bounding Boxes for Dense Object Detection," *Adv Neural Inf Process Syst*, vol. 33, pp. 21002–21012, 2020.
- [10] Z. Wei, C. Duan, X. Song, Y. Tian, and H. Wang, "AMRNet: Chips Augmentation in Aerial Images Object Detection," Sep. 2020, Accessed: Feb. 21, 2024. [Online]. Available: <https://arxiv.org/abs/2009.07168v2>
- [11] A. Inui *et al.*, "Detection of Elbow OCD in the Ultrasound Image by Artificial Intelligence Using YOLOv8," *Applied Sciences* 2023, Vol. 13, Page 7623, vol. 13, no. 13, p. 7623, Jun. 2023, <https://doi.org/10.3390/app13137623>
- [12] G. Yang, J. Wang, Z. Nie, H. Yang, and S. Yu, "A Lightweight YOLOv8 Tomato Detection Algorithm Combining Feature Enhancement and Attention," *Agronomy* 2023, Vol. 13, Page 1824, vol. 13, no. 7, p. 1824, Jul. 2023, <https://doi.org/10.3390/agronomy13071824>
- [13] D. Wang and L. Wang, "On OCT image classification via deep learning," *IEEE Photonics J*, vol. 11, no. 5, Oct. 2019, <https://doi.org/10.1109/JPHOT.2019.2934484>
- [14] T. Mahmood, M. Arsalan, M. Owais, M. B. Lee, and K. R. Park, "Artificial Intelligence-Based Mitosis Detection in Breast Cancer Histopathology Images Using Faster R-CNN and Deep CNNs," *Journal of Clinical Medicine* 2020, Vol. 9, Page 749, vol. 9, no. 3, p. 749, Mar. 2020, <https://doi.org/10.3390/jcm9030749>
- [15] M. Tripathi, "Analysis of Convolutional Neural Network based Image Classification Techniques," *Journal of Innovative Image Processing*, 2021, <https://doi.org/10.36548/jiip.2021.2.003>
- [16] Q. Liu, M. Wang, Z. Liu, B. Su, and N. Hanajima, "Defect Detection of Micro-Precision Glass Insulated Terminals," 2021, <https://doi.org/10.2991/jrnal.k.210521.005>
- [17] Y. Qian and F. Chen, "Optimization of Excess Bounding Boxes in Micro-part Detection and Segmentation," *Lecture Notes in Computer Science (including subseries Lecture Notes in Artificial Intelligence and Lecture Notes in Bioinformatics)*, vol. 11902 LNCS, pp. 738–749, 2019, https://doi.org/10.1007/978-3-030-34110-7_62
- [18] Y. Deng, "Uncertainty measure in evidence theory," *Science China Information Sciences*, vol. 63, no. 11, pp. 1–19, Nov. 2020, <https://doi.org/10.1007/s11432-020-3006-9>
- [19] J. Julian, F. Wahyuni, and F. D. Ulhaq, "Reliability Analysis of pH Measurement on TLC4502 with E201C Electrodes based on ATmega328P Microcontroller: Approach to Analysis of Variation with ANOVA,"

- ELKHA : Jurnal Teknik Elektro, vol. 15, no. 1, pp. 32–40, Apr. 2023, <https://doi.org/10.26418/elkha.v15i1.62982>
- [20] Kumari, Shruti, et al. "YOLOv8 Based Deep Learning Method for Potholes Detection." 2023 IEEE International Conference on Computer Vision and Machine Intelligence (CVMI). IEEE, 2023. <https://doi.org/10.1109/CVMI59935.2023.10465038>

